JACS
JOURNAL OF THE AMERICAN CHEMICAL SOCIETY

Communication

pubs.acs.org/JACS

Electrostatic Self-Assembling Formation of Pd Superlattice Nanowires from Surfactant-Free Ultrathin Pd Nanosheets

Chengyi Hu,[†] Kaiqiang Lin,[†] Xingli Wang,[†] Shengjie Liu,[†] Jun Yi,[†] Yu Tian,[‡] Binghui Wu,[†] Guangxu Chen,[†] Huayan Yang,[†] Yan Dai,[†] Huan Li,[†] and Nanfeng Zheng*[,†]

[†]State Key Laboratory for Physical Chemistry of Solid Surfaces, Collaborative Innovation Center of Chemistry for Energy Materials, and Department of Chemistry, College of Chemistry and Chemical Engineering, Xiamen University, Xiamen 361005, China

[‡]State Key Laboratory of Tribology, Tsinghua University, Beijing 100084, China

Supporting Information

ABSTRACT: A facile method has been developed for face-to-face assembly of two-dimensional surfactant-free Pd nanosheets into one-dimensional Pd superlattice nanowires. The length of the Pd nanowires can be well controlled by introducing cations of different concentration and charge density. Our studies reveal that cations with higher charge density have stronger charge-screening ability, and their introduction leads to more positive zeta-potential and decreased electrostatic repulsion between negatively charged Pd nanosheets. Moreover, their surfactant-free feature is of great importance in assembling the Pd nanosheets into superlattice nanowires. While the cations are important for the assembly of Pd nanosheets, the use of poly(vinylpyrrolidone) is necessary to enhance the stability of the assembled superlattice nanowires. The as-assembled segmented Pd nanowires display tunable surface plasmon resonance features and excellent hydrogen-sensing properties.

During the past decades, self-assembly of nanocrystals (NCs) has attracted considerable interest due to their wide range of applications in optics, electrics, catalysis, and sensing.[1] Various strategies have been developed to fabricate NC assemblies, such as interface induction,[2] gravitational sedimentation,[3] surface modification (e.g., CTAB and DNA),[4] and external-field assistance.[5] Taking advantages of these methods, one can construct various assembled structures by using NCs with different shapes as building blocks. Two-dimensional (2D) NCs are a kind of unique materials in self-assembly studies, because they can assemble either face-to-face, forming one-dimensional (1D) structures, or edge-to-edge, forming planar 2D structures.[6] Face-to-face stacked structures are thermodynamically favorable and have been observed in lanthanides[7] and semiconductor[8] nanoplates. Yet, when it comes to 2D metal NCs, the stacked assembled structure is rarely reported. Face-to-face self-assembly of Ag nanoplates was observed by the drop-casting method.[9] The hcp-Co nanodisks were assembled into 1D structures due to the magnetic interaction.[10]

To better understand the assembly behaviors of 2D metal NCs, the interparticulate interactions should be taken into consideration. In a colloidal solution of metal NCs, the predominant interactions are attributed to van der Waals force, electrostatic force, interaction between capping agents, and interaction between NCs and solvent. The attractive van der Waals force is usually balanced by electrostatic or steric repulsion; electrostatic repulsion comes from the charges on NCs, and the steric repulsion is provided by surfactants or polymers coated on the NCs.[11] Previous research showed that long-chain surfactants (e.g., CTAB and oleylamine) will promote the assembly due to van der Waals interactions between the surface ligands.[12] Yang et al. demonstrated that adsorbed poly(vinylpyrrolidone) (PVP) provided steric repulsion, and unadsorbed PVP in solution provided depletion attraction in the self-assembly of Ag superlattice;[3] still, capping agents will hinder the self-assembly in some cases. In 2002, Tang et al. found that CdTe nanoparticles self-assembled into nanowires upon removal of the excess organic stabilizer. They argued that partial stabilizer removal increased the dipole−dipole attraction between CdTe NCs.[13] Thus, the interaction between capping agents is rather complex and greatly interferes with other interparticulate interactions. To get a deeper understanding of interactions in self-assembly, we chose surfactant-free, negatively charged metal NCs to eliminate the influence of organic capping agents, where the electrostatic force would become predominant. Compared with the interaction between capping agents, the strength of electrostatic forces is much easier to control, providing us more opportunities to control the self-assembly,[14] but studies using 2D surfactant-free metal NCs as building blocks in self-assembly have been rarely reported.[15]

Herein, we demonstrate a facile strategy for assembling surfactant-free Pd nanosheets (NSs) into 1D Pd superlattice nanowires (SLNWs) by introducing trace amounts of counter-cations (e.g., Fe^{3+}, Al^{3+}). In the assembled structure, the Pd NSs are face-to-face stacked together to form SLNWs consisting of repeated Pd NSs and fixed gaps along the longitudinal direction. The concentration and charge density of introduced cations are two critical factors that control the assembling ability and the length of Pd SLNWs. Zeta-potential measurements reveal that the cations play an important role in shielding the negative charges on Pd NSs to decrease the electrostatic repulsion between them. Also, the surfactant-free feature of Pd NSs is important to achieve the face-to-face assembly. PVP, which is introduced after the assembly, serves as a scaffold to stabilize the Pd SLNWs. More interestingly, the assembled structures show a

Received: July 21, 2014
Published: August 29, 2014

   dx.doi.org/10.1021/ja507409p | J. Am. Chem. Soc. 2014, 136, 12856−12859

well-defined and tunable surface plasmon resonance (SPR) peak, which is rarely reported in the pure Pd system.[16] Owing to the 1D structure, the as-assembled Pd SLNWs exhibit excellent performance in sensing hydrogen gas (H_2).

Ultrathin Pd NSs without organic capping ligands on their surfaces were prepared using a carbonyl-mediated method recently developed by our group.[17] The surfactant-free feature has inspired us to further investigate their self-assembling behavior. As an oxidative etching agent, $FeCl_3$ was previously reported to have a significant influence on the growth process of the PVP-protected Pd NSs, resulting in the formation of mesocrystalline Pd nanocorolla.[18] We thus first introduced $FeCl_3$ in the room-temperature synthesis of surfactant-free Pd NSs (see the Supporting Information for details) to evaluate the influence of Fe^{3+}. To our surprise, 1D Pd SLNWs instead of mesocrystalline Pd nanocorolla were obtained.

To figure out the reason for the formation of 1D Pd SLNWs, we carefully characterized the as-prepared structure. As illustrated in the transmission electron microscopy (TEM) images (Figures 1a and S1), the SLNWs prepared with an Fe/Pd

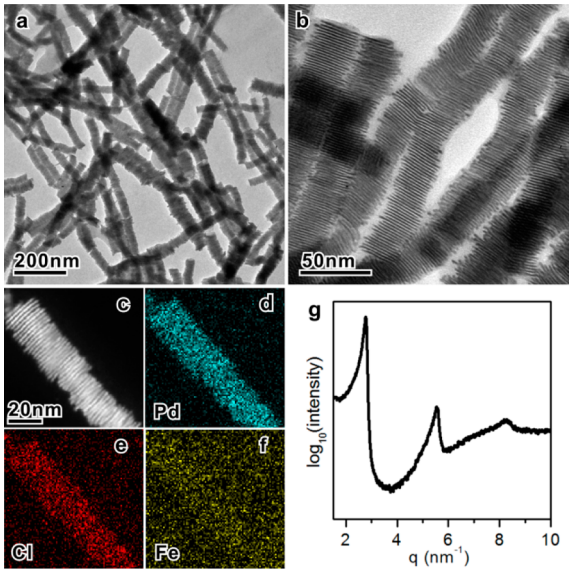

Figure 1. (a) Large-area and (b) enlarged TEM images, (c–f) HAADF-STEM-EDX mapping images, and (g) SAXS pattern of the as-prepared Pd SLNWs with an Fe^{3+}/Pd molar ratio of 1.

molar ratio of 1 had an average length of 283 nm and a diameter of 21 nm. The enlarged TEM image (Figure 1b) clearly shows that the Pd SLNWs were composed of periodically face-to-face assembled Pd NSs. High-angle annular dark field scanning transmission electron microscopy (HAADF-STEM) image and energy-dispersive X-ray (EDX) elemental mapping (Figure 1c–f) revealed that the structure consisted of Pd with Cl and small amounts of Fe on the surface. The negative-charged chloride ions provide electrostatic repulsion to stabilize the surfactant-free Pd NSs. As detected by inductively coupled plasma atomic emission spectroscopy (ICP-AES), there was ~1% of Fe in the products. To get a deeper understanding of this structure, Pd SLNWs in the as-made solution were characterized using small-angle X-ray scattering (SAXS). As shown in Figure 1g, the periodicity in the SAXS patterns, with three peaks at q = 2.76, 5.52, and 8.28 nm^{-1}, indicated the presence of Pd SLNWs in the solution rather than their formation by evaporating the solvent on a TEM grid. The position of the first peak in the SAXS patterns corresponds to a

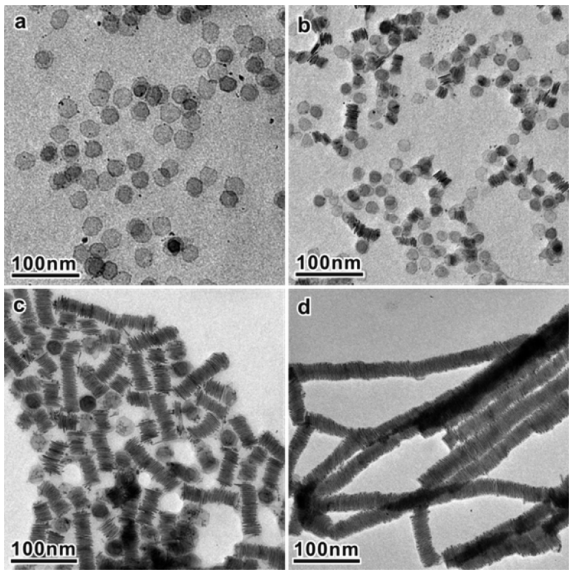

Figure 2. TEM images of Pd NSs (a) and Pd SLNWs (b–d) obtained at different Fe^{3+}/Pd molar ratios: (b) 0.02, (c) 0.05, and (d) 0.1. Increasing the amount of $FeCl_3$ promoted the assembly of Pd NSs to form longer SLNWs.

2.3 nm of center-to-center distance between the two nearest Pd NSs ($d = 2\pi/q$),[19] in accordance with the TEM results.

The use of $FeCl_3$ is of critical importance for the self-assembly. The length of Pd SLNWs can be finely controlled by regulating the concentration of $FeCl_3$. In the absence of $FeCl_3$, the products were freestanding Pd NSs (Figure 2a). When the molar ratio of Fe/Pd reached 0.02, Pd NSs began to assemble into short nanorods with lengths of 25 ± 6 nm (Figure 2b). As the Fe/Pd ratio was gradually increased to 0.05, 0.1 and 1, the average length of Pd SLNWs increased from 63 to 168 and 283 nm, respectively (Figures 2c,d and S1, and Table S1). When the $FeCl_3$ concentration was further increased, the products were precipitated out due to the high ionic strength. When the Fe/Pd ratio was further decreased to 0.01, the Pd NSs were not able to assemble (Figure S4a). With the increasing length, the diameters of the Pd SLNWs were always identical with those of the Pd NSs (Table S1), further confirming that the Pd NSs served as the building blocks. Pd SLNWs of different lengths showed identical SAXS patterns as well, indicating that the average gap distance was at the same value (Figure S5). Since CO binds strongly on both the upper and lower (111) surfaces of the Pd NSs,[16a] we thus consider that CO binding is the main reason for forming the gaps. To see whether the Cl^- ions in $FeCl_3$ are necessary for the self-assembly process, $FeCl_3$ was replaced by the same amount of $Fe(NO)_3$.The Pd NSs were able to assemble into SLNWs as well (Figure S4b). It can be thus concluded that Fe^{3+} cations determine the assembling ability of Pd NSs, and increasing the concentration of Fe^{3+} cations facilitates their assembly to form longer Pd SLNWs.

To get a deeper understanding of why Fe^{3+} cations promoted the assembly, the interactions between Pd NSs were taken into consideration. Electrostatic control of the self-assembly of NCs has been widely studied,[20] but most of the experiments were performed on surfactant-capped NCs. The presence of interactions between capping agents greatly interferes with the overall assembly behaviors of surfactant-capped NCs. Thus, we first investigated how cations influence the electrostatic interactions between surfactant-free Pd NSs. As revealed by ζ-

dx.doi.org/10.1021/ja507409p | J. Am. Chem. Soc. 2014, 136, 12856–12859

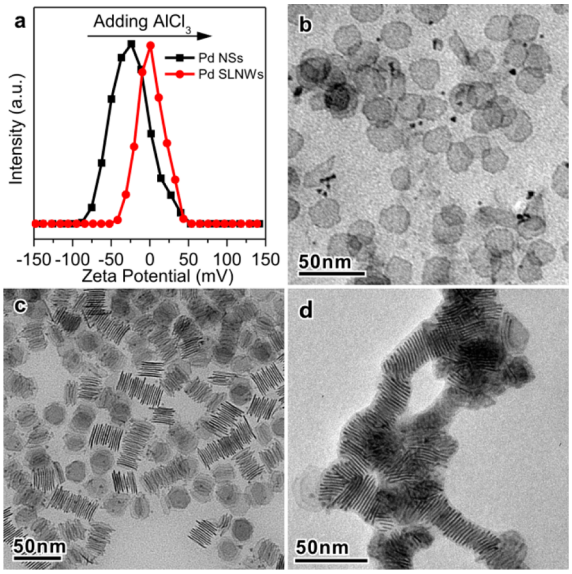

Figure 3. (a) Zeta-potentials of the Pd NSs before addition of $AlCl_3$ and of the Pd SLNWs after addition of $AlCl_3$, measured in the original DMF solution. (b–d) TEM images of Pd NSs or SLNWs prepared with NaCl (b), $MgCl_2$ (c), and $AlCl_3$ (d) aqueous solution under the same ionic strength of 3.6 mM.

potential measurements (Figure 3a), the Pd NSs were negatively charged in DMF solution. Upon addition of 10 μL of $AlCl_3$ aqueous solution (Al/Pd = 0.01), the charge changed to almost zero, and the Pd NSs assembled at the same time (Figure S4c). We propose that the countercations shield the negative charges on Pd NSs, and thus electrostatic repulsion is greatly reduced, leading to the assembly of Pd NSs into SLNWs.

From the above analysis, it is expected that other charged species can also induce self-assembly. Research in biophysics has shown nicely that the self-assembly of biomolecules follows the theory of counterion condensation.[21] The folding efficiency of RNA can be greatly improved by using divalent cations to replace monovalent cations.[22] Inspired by these results, we chose NaCl, $MgCl_2$, and $AlCl_3$ to investigate the influence of cations' valence. As shown in Figure 3b–d, under the same ionic strength of 3.6 mM, trivalent Al^{3+} cations were able to assemble the Pd NSs together into reasonably long SLNWs, but monovalent Na^+ cations were not. The divalent Mg^{2+} cations assembled Pd NSs into short nanorods. The ζ-potential measurements (Table S2) revealed that cations with higher valence led to more positive ζ-potentials under the same ionic strength. With increasing concentration, the ζ-potential moved toward positive values, but to different extents. The ζ-potential was still quite negative even in the presence of a high concentration of Na^+, which was not able to induce self-assembly (Figure S6a). In comparison, the ζ-potential in the presence of Mg^{2+} moved to a more positive value than Na^+. Increasing the Mg^{2+} concentration readily induced self-assembly to form longer SLNWs (Figure S6b). In the case of Al^{3+}, the ζ-potential did not increase further when the ionic strength increased above 36 mM since all of the Pd NSs were assembled into SLNWs. To better explain this phenomenon, we introduced the charge density ($\rho = Ze/V$) to describe the charge-screening ability of countercations, where Z is the valence, e is the elementary charge, and V is the volume of cations.[23] The charge densities of different cations were calculated (Table S3). The results showed that the charge densities of trivalent cations were much higher than those of divalent and monovalent cations. Thus, trivalent cations showed the largest ability to assemble Pd NS under the same ionic strength. Thus, both the concentration and the charge density of cations influence the surface charge of Pd NSs. A more positive ζ-potential resulted in the formation of longer Pd SLNWs.

Countercations play important roles in the self-assembly of Pd NSs. It should be noted that PVP is also necessary in forming stable Pd SLNWs. In this work, PVP was introduced after the assembly, so the effect was rather different from that in the previous studies.[3] To better understand the role of PVP, the original products without added PVP was characterized by TEM; the images showed that Pd SLNWs did exist (Figure S7a,b). However, when the excess salts were removed by washing, the Pd SLNWs were destroyed during the centrifugation or ultrasonic dissolution (Figure S7c). If some PVP was introduced into the solution after the assembly but before the purification, the Pd SLNWs were nicely preserved. When PVP was introduced before $FeCl_3$, it adsorbed on the surface of Pd NSs and prevented the assembly (Figure S7e). It should be noted that, although the face-to-face assembly was also observed on Pd NSs prepared in the co-presence of cetyltrimethylammonium bromide (CTAB) and PVP,[16a] the assembled structures were much shorter than Pd SLNWs assembled from surfactant-free Pd NSs (Figure S8). The absence of surfactants is a key factor for the self-assembly of Pd NSs into long Pd SLNWs, yet it is obvious that PVP serves as a scaffold to increase the stability of the final assembled structure.[24]

The most exciting feature of the as-assembled Pd SLNWs is that they exhibit well-defined and tunable SPR properties. As shown in Figure 4a, the extinction spectra experienced a great

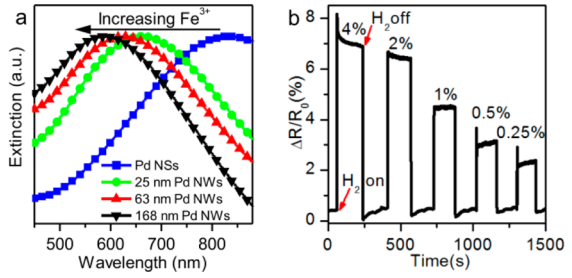

Figure 4. (a) UV–vis extinction spectra of the Pd NSs and Pd SLNWs. The SPR peak blue-shifted with increasing length. (b) Change in the resistance of Pd SLNWs upon exposure to H_2 gas at different concentrations.

blue-shift during the assembly. The Pd NSs with an average diameter of 21 nm had a SPR peak at 838 nm. The extinction peak of the Pd SLNWs shifted from 660 to 623 and 590 nm with increasing length. To explain the shift of the SPR peak, we calculated the extinction spectra using the discrete dipole approximation method.[25] As shown in Figure S9, the SPR peak showed a surprisingly large blue-shift while more and more Pd NSs were stacked, qualitatively matching with the experimental results. The calculated incident direction-dependent extinction spectra indicate that the plasmonic absorption comes from the in-plane mode rather than the out-of-plane mode of Pd SLNWs (Figure S10), which is different from the case of Ag nanoplates.[9] To better understand the SPR property, the charge distribution of Pd SLNWs was calculated under the peak wavelength (Figure S11). The in-phase repulsive charge distribution corresponded to an antibonding mode[26] according to the plasmon hybridization theory,[27] resulting in the large blue-shift. As the plasmon coupling is sensitive to the interparticulate distance, the decrease

dx.doi.org/10.1021/ja507409p | J. Am. Chem. Soc. 2014, 136, 12856–12859

of gap size will result in the larger blue-shift in antibonding mode, which is confirmed by the calculation (Figure S12). Thus, the blue-shift of the SPR peak during assembly is due to the repulsive charge distribution between stacked Pd NSs caused by in-plane plasmon coupling. This large blue-shift and unique interacting mode are rarely reported in the literature.

In addition to the unique SPR property, the assembled Pd SLNWs exhibited excellent performance in H_2 sensing due to the 1D assembly structure and the ultrathin nature of the Pd NSs (Figure 4b). Before the measurement, a suspension of Pd SLNWs was dropped on the interdigital electrodes. Exposure of the assembled Pd SLNWs to H_2 gas at room temperature caused a rapid and reversible increase of the resistance, due to the formation of PdH_x.[28] As the concentration of H_2 gas decreased from 4% to 0.25% with argon as the carrier gas, the change of resistance ($\Delta R/R_0$) decreased from ~7% to 2%. No obvious change of morphology was observed after exposure to H_2, indicating the excellent stability and reversibility of Pd SLNWs (Figure S13).

In conclusion, a facile method has been developed to assemble 2D surfactant-free Pd NSs into 1D SLNWs by inducing cations to regulate the electrostatic interaction. The efficacy for trivalent cations to induce the assembly was much higher than for divalent cations and individual monovalent cations. Both the concentration and charge density of cations influenced the surface charge of Pd NSs by shielding negative charges on the Pd NSs, thus decreasing the repulsive electrostatic interaction between NSs. A more positive ζ-potential resulted in the formation of longer Pd SLNWs. The surfactant-free feature of Pd NSs eliminates the influence of interactions between capping agents, ensuring self-assembly under electrostatic control. The as-assembled Pd SLNWs had well-defined and tunable SPR feature. We attribute the extremely large blue-shift during assembly to the unique ultrathin feature and ultrasmall separation (~1 nm) between the Pd NSs, which cause strong in-plane plasmon coupling. Moreover, the as-assembled Pd SLNWs exhibited excellent performance in H_2 sensing. We believe that this cation-induced charge-screening method can be used to assemble other surfactant-free NCs. The Pd SLNWs with sub-nanometer gaps are expected to provide an excellent model for molecular electronics to study the tunneling behavior of electrons.

■ ASSOCIATED CONTENT

Supporting Information

Experimental details and additional data, including Figures S1−S13 and Tables S1−S3. This material is available free of charge via the Internet at http://pubs.acs.org.

■ AUTHOR INFORMATION

Corresponding Author

nfzheng@xmu.edu.cn

Notes

The authors declare no competing financial interest.

■ ACKNOWLEDGMENTS

We thank colleagues for helpful discussions: Z. L. Yang for SPR calculations, B. Liu for H_2 sensing, and L. Gu and H.G. Liao for HRTEM characterizations. We thank the MOST of China (2011CB932403, 2014CB932004), the NSFC (21131005, 21333008, 21420102001), and the NFFTBS (J1310024) for financial support.

■ REFERENCES

(1) (a) Rycenga, M.; Cobley, C. M.; Zeng, J.; Li, W. Y.; Moran, C. H.; Zhang, Q.; Qin, D.; Xia, Y. N. *Chem. Rev.* **2011**, *111*, 3669. (b) Gong, J.; Li, G.; Tang, Z. *Nano Today* **2012**, *7*, 564. (c) Shibu, E. S.; Muhammed, M. A. H.; Kimura, K.; Pradeep, T. *Nano Res.* **2009**, *2*, 220. (d) Urban, J. J.; Talapin, D. V.; Shevchenko, E. V.; Kagan, C. R.; Murray, C. B. *Nat. Mater.* **2007**, *6*, 115. (e) Yamada, Y.; Tsung, C. K.; Huang, W.; Huo, Z. Y.; Habas, S. E.; Soejima, T.; Aliaga, C. E.; Somorjai, G. A.; Yang, P. D. *Nat. Chem.* **2011**, *3*, 372. (f) Anker, J. N.; Hall, W. P.; Lyandres, O.; Shah, N. C.; Zhao, J.; Van Duyne, R. P. *Nat. Mater.* **2008**, *7*, 442.

(2) Dong, A. G.; Chen, J.; Vora, P. M.; Kikkawa, J. M.; Murray, C. B. *Nature* **2010**, *466*, 474.

(3) Henzie, J.; Grunwald, M.; Widmer-Cooper, A.; Geissler, P. L.; Yang, P. D. *Nat. Mater.* **2012**, *11*, 131.

(4) (a) Nie, Z. H.; Fava, D.; Kumacheva, E.; Zou, S.; Walker, G. C.; Rubinstein, M. *Nat. Mater.* **2007**, *6*, 609. (b) Jones, M. R.; Macfarlane, R. J.; Lee, B.; Zhang, J. A.; Young, K. L.; Senesi, A. J.; Mirkin, C. A. *Nat. Mater.* **2010**, *9*, 913. (c) Wang, P. P.; Yu, Q. Y.; Long, Y.; Hu, S.; Zhuang, J.; Wang, X. *Nano Res.* **2012**, *5*, 283.

(5) Ryan, K. M.; Mastroianni, A.; Stancil, K. A.; Liu, H. T.; Alivisatos, A. P. *Nano Lett.* **2006**, *6*, 1479.

(6) Ye, X. C.; Chen, J.; Engel, M.; Millan, J. A.; Li, W. B.; Qi, L.; Xing, G. Z.; Collins, J. E.; Kagan, C. R.; Li, J.; Glotzer, S. C.; Murray, C. B. *Nat. Chem.* **2013**, *5*, 466.

(7) Zhao, F.; Yuan, M.; Zhang, W.; Gao, S. *J. Am. Chem. Soc.* **2006**, *128*, 11758.

(8) Sigman, M. B.; Ghezelbash, A.; Hanrath, T.; Saunders, A. E.; Lee, F.; Korgel, B. A. *J. Am. Chem. Soc.* **2003**, *125*, 16050.

(9) Bae, Y.; Kim, N. H.; Kim, M.; Lee, K. Y.; Han, S. W. *J. Am. Chem. Soc.* **2008**, *130*, 5432.

(10) Puntes, V. F.; Zanchet, D.; Erdonmez, C. K.; Alivisatos, A. P. *J. Am. Chem. Soc.* **2002**, *124*, 12874.

(11) Min, Y. J.; Akbulut, M.; Kristiansen, K.; Golan, Y.; Israelachvili, J. *Nat. Mater.* **2008**, *7*, 527.

(12) Du, Y. P.; Zhang, Y. W.; Sun, L. D.; Yan, C. H. *J. Am. Chem. Soc.* **2009**, *131*, 3162.

(13) Tang, Z. Y.; Kotov, N. A.; Giersig, M. *Science* **2002**, *297*, 237.

(14) Walker, D. A.; Kowalczyk, B.; de la Cruz, M. O.; Grzybowski, B. A. *Nanoscale* **2011**, *3*, 1316.

(15) Hou, C. P.; Zhu, J.; Liu, C.; Wang, X.; Kuang, Q.; Zheng, L. S. *CrystEngComm* **2013**, *15*, 6127.

(16) (a) Huang, X. Q.; Tang, S. H.; Mu, X. L.; Dai, Y.; Chen, G. X.; Zhou, Z. Y.; Ruan, F. X.; Yang, Z. L.; Zheng, N. F. *Nat. Nanotechnol.* **2011**, *6*, 28. (b) Niu, Z. Q.; Zhen, Y. R.; Gong, M.; Peng, Q.; Nordlander, P.; Li, Y. D. *Chem. Sci.* **2011**, *2*, 2392.

(17) Li, H.; Chen, G. X.; Yang, H. Y.; Wang, X. L.; Liang, J. H.; Liu, P. X.; Chen, M.; Zheng, N. F. *Angew. Chem., Int. Ed.* **2013**, *52*, 8368.

(18) Huang, X. Q.; Tang, S. H.; Yang, J.; Tan, Y. M.; Zheng, N. F. *J. Am. Chem. Soc.* **2011**, *133*, 15946.

(19) Paik, T.; Ko, D. K.; Gordon, T. R.; Doan-Nguyen, V.; Murray, C. B. *ACS Nano* **2011**, *5*, 8322.

(20) (a) Zhang, H.; Wang, D. Y. *Angew. Chem., Int. Ed.* **2008**, *47*, 3984. (b) Liu, Y. Z.; Lin, X. M.; Sun, Y. G.; Rajh, T. *J. Am. Chem. Soc.* **2013**, *135*, 3764. (c) Li, W. Y.; Camargo, P. H. C.; Au, L.; Zhang, Q.; Rycenga, M.; Xia, Y. N. *Angew. Chem., Int. Ed.* **2010**, *49*, 164.

(21) Wong, G. C. L.; Pollack, L. *Annu. Rev. Phys. Chem.* **2010**, *61*, 171.

(22) Heilman-Miller, S. L.; Thirumalai, D.; Woodson, S. A. *J. Mol. Biol.* **2001**, *306*, 1157.

(23) Koculi, E.; Hyeon, C.; Thirumalai, D.; Woodson, S. A. *J. Am. Chem. Soc.* **2007**, *129*, 2676.

(24) Maheshwari, V.; Kane, J.; Saraf, R. F. *Adv. Mater.* **2008**, *20*, 284.

(25) Draine, B. T.; Flatau, P. J. *J. Opt. Soc. Am. A* **1994**, *11*, 1491.

(26) Chang, Y. C.; Wang, S. M.; Chung, H. C.; Tseng, C. B.; Chang, S. H. *ACS Nano* **2012**, *6*, 3390.

(27) Prodan, E.; Radloff, C.; Halas, N. J.; Nordlander, P. *Science* **2003**, *302*, 419.

(28) Yang, F.; Kung, S. C.; Cheng, M.; Hemminger, J. C.; Penner, R. M. *ACS Nano* **2010**, *4*, 5233.